New insights into the convective and microphysical characteristics of heavy rainfall in monsoon coastal areas (South China)

YALI LUO#,*, YANYU GAO# and YANGRUIXUE CHEN**

#State Key Laboratory of Severe Weather, Chinese Academy of Meteorological Sciences, Beijing 100081, China

*Collaborative Innovation Center on Forecast and Evaluation of Meteorological Disasters,

Nanjing University of Information Science and Technology, Nanjing 210044, China

**School of Atmospheric Sciences, Chengdu University of Information Technology, Chengdu 610225, China

e mail : ruixue@cuit.edu.cn

सार – पिछले तीन वर्षों के दौरान, दक्षिण चीन जो कि एक प्रतिरुपी मॉनसूनी तटीय क्षेत्र है, में भारी वर्षा केसंवहनीय गुणों और सूक्ष्म भौतिकीय विशेषताओं में नई जानकारी प्राप्त हुई है। इस तरह की बेहतर समझ उन्नत सुदूर संवेदी तकनीकों के अनुप्रयोग की तीव्र प्रगति और दक्षिण चीन में परिचालनात्मक मौसम रेडारों के दोहरे-ध्रुवण कार्य के उन्नयन से संबंधित है। इस लेख में लगभग 2019 के बाद से तीन पहलुओं में प्रतिनिधि अध्ययनों की समीक्षा की गई है। पहला, उष्म ऋतु मौसम के दौरान संवहन आरंभ होने के स्थानों कास्थानिक कालिक वितरण और दैनिक प्रसार। दूसरा, पूर्वग्रीष्मकालीन वर्षाऋतु (अप्रैल से जून) के दौरान मेसो-β-स्केल संवहन प्रणालियों (MCS) की सामान्य विशेषताएं और सिनोप्टिक-स्केल वातावरण। तीसरा, दक्षिण चीन मेंअत्यधिक अल्पकालिक वर्षा की सूक्ष्म भौतिक विशेषताएं और समीपवर्तीवाताग्र तथाउष्म क्षेत्र में भारी वर्षा।

ABSTRACT. During the past three years, new insights have been gained into the convective features and microphysical characteristics of heavy rainfall in South China, which is a typical monsoon coastal area. Such improved understanding is closely related to the rapid progress of application of advanced remote sensing techniques, in particular the upgrade of the dual-polarization function of the operational weather radars in South China. This paper reviews the representative studies since approximately 2019 in three aspects. First, spatiotemporal distribution and diurnal propagation of the convection initiation during the warm season. Second, general features and synoptic-scale environments of the meso-β-scale convective systems (MCSs) during the pre-summer rainy season (April to June). Third, microphysical characteristics of the extreme short-term rainfall and the coexisting frontal and warm-sector heavy rainfall in South China.

Key words – Radar climatology of convection initiation, South China.

1. Introduction

Heavy rainfall is produced frequently in the Asian summer monsoon region, particularly in coastal areas, mostly by moist convection (Houze *et al*., 2007; Xie *et al*., 2006). One of the monsoon coastal areas is South China. It is located in the north of the South China Sea (SCS) and east of the Tibetan Plateau, with an urban agglomeration in the Pearl River Delta (PRD) facing the SCS to the southeast and surrounded by mountains on the other sides [Fig. 1(a)]. The heavy rainfall over South China occurs from April to early October (Ramage, 1952) and

occasionally cause severe floods, landslides and urban water logging that may result in serious disasters. The rainy season in South China can be divided into two stages, *i.e*., the earlier and later rainy seasons, with mid to late June as the dividing point (Yuan F. *et al*., 2010). This is in accordance with the sub-seasonal march of the east Asian summer monsoon (EASM) circulation and rainfall (Qian and Lee, 2000; Chen *et al*., 2004; Ding and Chan, 2005).

Heavy rainfall during the earlier rainy season of South China (April to June; also referred to as the pre-

summer rainy season) has been extensively studied since the 1980s (Huang *et al*., 1986; Zhou *et al*., 2003; Ni and Zhou, 2006; Zhang *et al*., 2011; Luo *et al*., 2017). These studies have not only advanced the scientific understanding of heavy rainfall, but also promoted the development of techniques for its monitoring and prediction. More rapid progress in the relevant sciences and technologies has been achieved after entering the 21st century, partially due to the rapid economic development in China. Luo *et al*. (2020) comprehensively summarized the research papers (mostly published during 2008-2018) related to the pre-summer rainfall over South China, including the climatology of precipitation, relation between heavy rainfall and multi-scale physical processes and numerical weather prediction (NWP) studies. A concise description of current understanding of features and mechanisms of the heavy rainfall and related convection is provided here for brevity.

The per-summer heavy rainfalls in South China can be categorized into frontal and warm-sector heavy rainfall in literature. The frontal heavy rainfall (FR) is near the synoptic-scale cold front established by the convergence of cold-dry-northerly airflows and warm-moist-southerly airflows (Ding, 1994). The warm-sector heavy rainfall (WR) occurs more than 200 km ahead of the front in the warm sector without obvious synoptic lifting (Huang *et al*., 1986), mostly near the coastlines (Wu *et al*., 2020) and around the city agglomeration (Luo *et al*., 2020). While the FR is distributed quite extensively over inland areas of South China, the WR is more localized, but more intense in association with more favorable thermodynamical conditions. Convection initialization and development of the WR in South China are closely related to deceleration of the southerly marine boundary layer (BL) flows approaching South China (Li *et al*., 2020; Du *et al*., 2020b; Bao *et al*., 2021), topographic lifting (Wang *et al.*, 2014; Du *et al*., 2020a), cold pools (Wu and Luo, 2016), land-sea contrasts (Wu *et al*., 2020) and the synergetic interactions between urban-induced circulation (Shepherd, 2005) and some disturbances of synoptic-scale and mesoscale (Wu *et al*., 2019; Yin *et al*., 2020; Sun *et al*., 2021). At least two distinct organizational modes of rainstorms at their mature stage are observed in some extreme WR events, which had the maximum hourly rainfall above 100 or even 200 mm and the maximum rainfall accumulation in several hours beyond 300 or even 500 mm. One is the "band training" of several parallel rainbands that move eastward slowly, with each of the rainbands consisting of "echo training" of convective cells (Wang *et al*., 2014; Wu and Luo, 2016; Liu *et al*., 2018). The other has a meso-γ-scale, circular convective core embedded in a meso-β-scale storm that exhibits a less obvious band structure (Li *et al*., 2021; Yin *et al*., 2020; Zeng and Wang, 2022).

Heavy rainfall over South China during the later rainy season (roughly July-September) is mainly produced under the influence of monsoonal troughs and lows (Huang *et al*., 2005), tropical cyclones (Meng and Wang, 2016) and the intraseasonal oscillation of the SCS summer monsoon (Hong and Ren, 2013).

This article aims to review the most recent (since approximately, 2019) research progress about convective and microphysical characteristics of heavy rainfall in South China during the warm season, which are obtained mainly based on the newly established dual-polarimetric radar network combined with other remote sensors such as disdrometers. The layout of the paper is as follows: the spatiotemporal distributions of convection initiation (CI) during the warm season (April to September) and meso-β-scale convective systems (MCSs) during the pre-summer rainy season will be described in Sections 2 and 3, respectively; section 4 will present microphysical characteristics of heavy rainfall, including a comparison between coexisting WR and FR in a heavy rainfall event and the statistics of extreme short-term rainfall accumulation in two warm seasons; finally concluding remarks are given in Section 5.

2. A radar climatology of Convection Initiation (CI) in South China

A CI climatology is valuable to understand convection triggering processes. However, such a climatology is not yet available in most monsoon coastal areas. To generate long-term CI statistics in South China, Bai *et al*. (2020a,b) utilized radar reflectivity derived from high-quality radar mosaic maps operationally produced by the China Meteorological Administration (CMA) during the warm seasons of 2013 to 2019 to identify CI events. The data has a spatial resolution of approximately 2.15 km and is available every 10 min before 15th June, 2016 and every 6 min afterward. A CI event is defined as the first occurrence of a convective cell (≥40 dBZ) when at least one of the following conditions is met: (*i*) No pixel exceeding 25 dBZ was observed 30 min prior to the candidate convective cell within 60 km of the current position of the cell, or (*ii*) no pixel reaching 35 dBZ was observed 30 min prior to the candidate convective cell within 60 km of the current position of the cell and no pixel exceeding 25 dBZ was observed 60 min prior to the candidate convective cell within 100 km of the current position of the cell (Bai *et al*., 2020a). Thus, the identified CI is associated with locally developed new convection. The authors obtained nearly 25,600 CI events and derived the first long-term CI climatology on monsoon coasts.

It was found that, almost 60% of CI events are concentrated within 100 km of the coastline, while
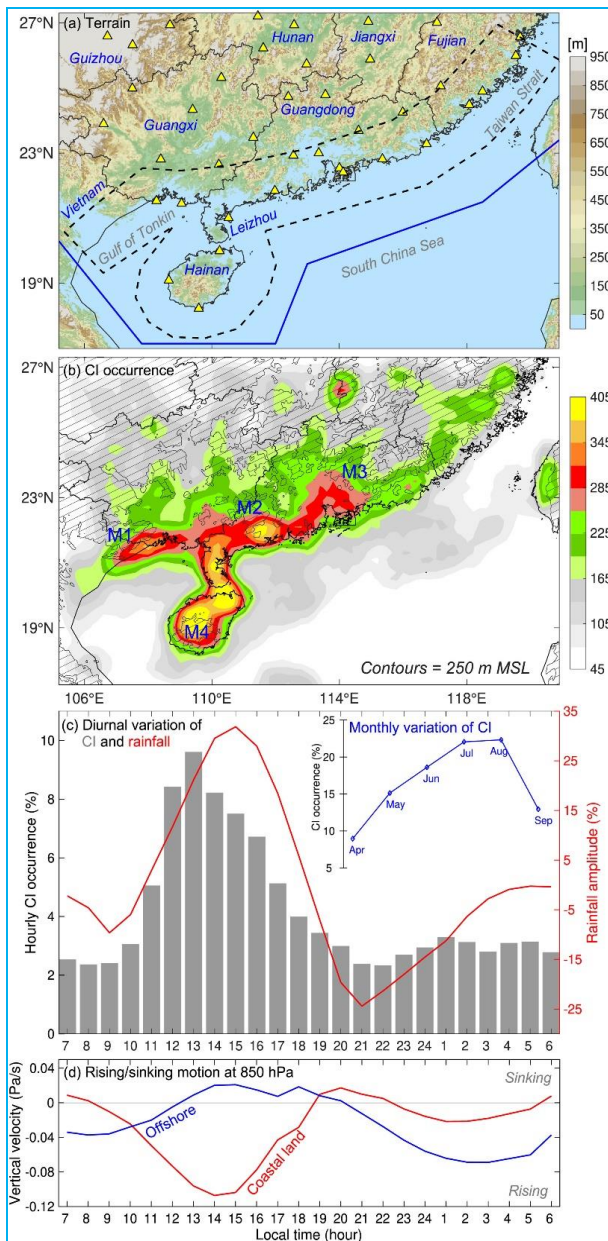
Figs. 1(a-d). (a) Terrain heights (units: m) with radar sites (triangles). (b) Density number (shaded) and (c) diurnal (gray) and monthly (blue) variations of CI occurrence during April-September from 2013 to 2019. In panel (b), the mountains labeled M1, M2, M3 and M4 are described in the text. The hatched area within the contours indicates the terrain at an altitude of 250 m. In panel (c), the diurnal variation of rainfall amplitude (red) is derived from the CMORPH data during April-September from 2013 to 2018, which is averaged in the domain to the north of the blue line in panel (a). The diurnal and monthly variations of CI occurrence were estimated by counting all the CI samples shown in panel (b). (d) Diurnal variation of averaged vertical velocity (units: Pa s^{-1}) at 850 hPa calculated within the dashed black polygon in panel (a) using the ERA5 data during April-September from 2013 to 2019. Adapted from Bai *et al.* (2020a)
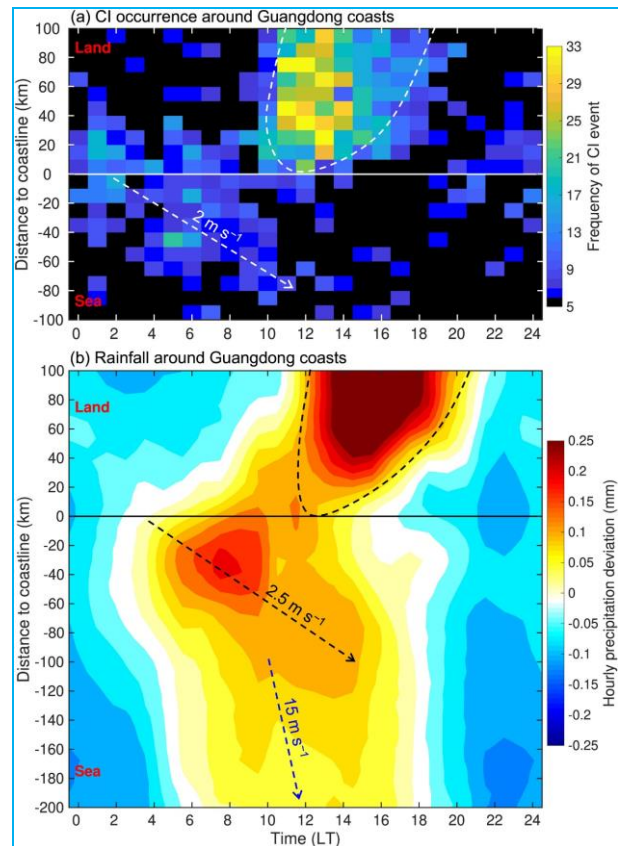
Figs. 2(a&b). Distance-time Hovmöller diagrams of (a) coastal CI occurrences and (b) hourly CMORPH rainfall deviations (the rainfall rate at the current hour minus the mean rainfall rate throughout the day) around the Guangdong coasts [refer to the blue box in Fig. 4(b) of Bai *et al.* (2020b)]. The CI occurrences in panel (a) are identified during April-September from 2013 to 2019. The CI occurrence in the far offshore is not shown for much fewer CI samples in that region. The hourly rainfall deviations in panel (b) are calculated during April-September from 2013 to 2018. The dashed ellipses outline the CI (rainfall) areas with relatively strong signals on land. The dashed arrows indicate the rough directions of offshore propagation described in the text. Adapted from Bai *et al.* (2020b)

offshore CI occurrences are much fewer than those on the near-coast land in South China [Fig. 1(b)]. Several CI hotspots are situated adjacent to mountains in the coastal regions (M1 to M3) and the tropical islands and peninsula (M4), suggesting great influences of topography and sea-land contrasts on the CI. The sub-seasonal variation of CI in South China is strongly affected by the summer monsoon. The occurrence frequency of CI increases sharply after the monsoon onset in May and reaches a maximum in July and August [see the inset in Fig. 1(c)], due to the warm moist air and associated convective instability brought by the summer monsoonal flows, favoring the widespread presence of CI events in South

China. Moreover, the diurnal variation of CI is strongly regulated by both large-scale vertical motion and land-ocean breeze circulation that is driven by solar heating. About 65% of CI events occur during daytime hours (07−19 LT; LT = UTC + 8 h) with a strong increase from 10 local time (LT; LT = 8h + UTC) and peak at 13 LT. The CI occurrence and offshore (coastal land) updraft, when averaged over the coastal land and near-offshore areas (the dashed black polygon in Fig. 1(a), increase simultaneously during 21−02 LT (10−13 LT), indicating a good consistency between the CI and the regional-scale vertical motion [Figs. 1(c&d)].

The characteristic of CI's near-offshore spread prior to rainfall in South China was illuminated for the first time by Bai *et al.* (2020a). For the near-offshore (<100 km away from coastline) CI, a seaward propagating feature was found after midnight, which precedes the rainfall propagation by 2-3 hr [Figs. 2(a&b)]. The slow propagation of CI occurrence is comparable to that of rainfall near-offshore (refer to the white (black) arrows in Figs. 2(a&b). The speed of far offshore (>100 km away from coastline) rainfall propagation is much higher than that of near-offshore speeds, due to gravity waves (Aves and Johnson, 2008). Previous studies have demonstrated that CI tends to coincide with a nocturnal low-level convergence, which is usually maximized near the sea due to land breeze and onshore monsoon flow (Houze *et al.*, 1981; Chen *et al.*, 2016; Chen *et al.*, 2018; Li *et al.*, 2019) and CI always occurs before convection-induced processes, such as cold pools. Thus, Bai *et al.* (2020a) speculated that the CI's near-offshore propagation characteristic is affected by the offshore land breezes or down slope wind, rather than the far offshore gravity wave.

3. General features of pre-summer MCSs

MCSs are major producers of heavy rainfall in many regions worldwide (Roca *et al.*, 2014; Virts and Houze Jr., 2016; Houze Jr., 2018; Schumacher and Rasmussen, 2020) including South China (Xu *et al.*, 2009; Luo *et al.*, 2013). However, the general features of MCSs in South China had not been clear until the study of Chen *et al.* (2022). They defined an MCS as a contiguous area of strong radar reflectivity (≥ 40 dBZ) extending at least 100 km in any horizontal direction and lasting no less than 3 h, following previous studies, *e.g.*, Parker and Johnson (2000). Therefore, the MCSs are of the meso-*β*-scale. During the lifespan of an MCS, its initiation time was defined as the time when the first echo is greater than 40 dBZ and its formation time was defined as the time when a contiguous area of strong reflectivity (≥ 40 dBZ) extending to at least 100 km in any horizontal direction of the MCS was first observed. With such definitions, 98 MCSs and their evolution details were identified during
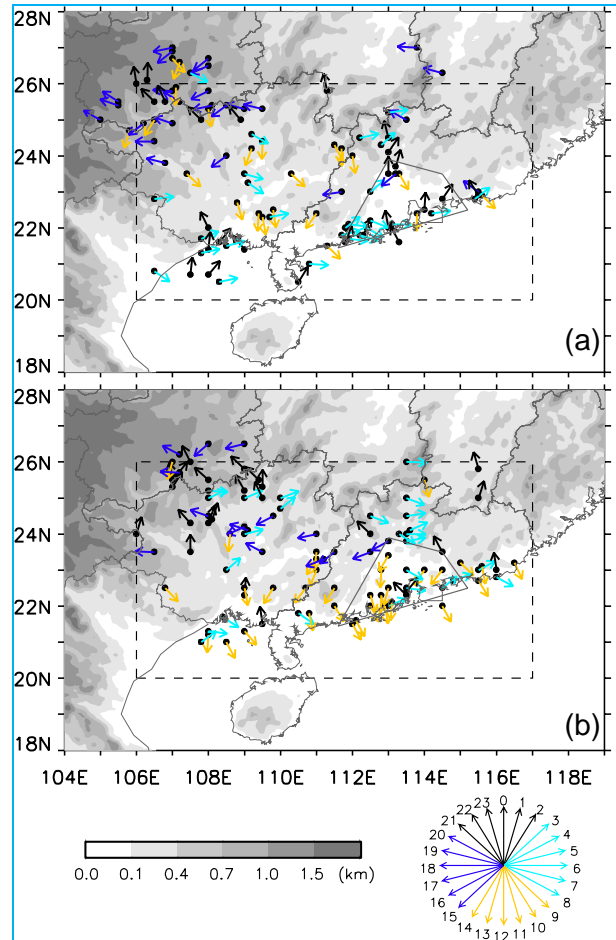
Figs. 3(a&b). The time (LT) (colored arrows) and location of the MCSs' (a) initiation and (b) formation. The grey scale shading denotes the terrain, the grey lines indicate the provincial boundaries and coastlines, the grey irregular quadrilateral demonstrates the Pearl River Delta region and the dashed rectangle denotes the analysis region of this study. Reprinted from Chen *et al.* (2022), copyright 2022, with permission from Elsevier

May 1-June 15, 2013-2017. Then, the spatial and temporal distribution characteristics of the initiation and formation time of a large number of MCSs observed during the pre-summer rainy season were shown by Chen *et al.* (2022) [Figs. 3(a&b)]. There are three high-frequency sub regions of MCS formation over South China, namely, North Guangxi (N-GX), South Guangxi (S-GX) and the Pearl River Delta (PRD), respectively. On average, the location of MCS initiation [Fig. 3(a)] is about 1 degree west and/or north of the location of MCS formation [Fig. 3(b)]. The formation time of MCSs is delayed by about 4.9 hours compared with the time of MCS initiation, which is comparable to that of the squall line over southeast China (4.7 hours; Meng *et al.*, 2013).
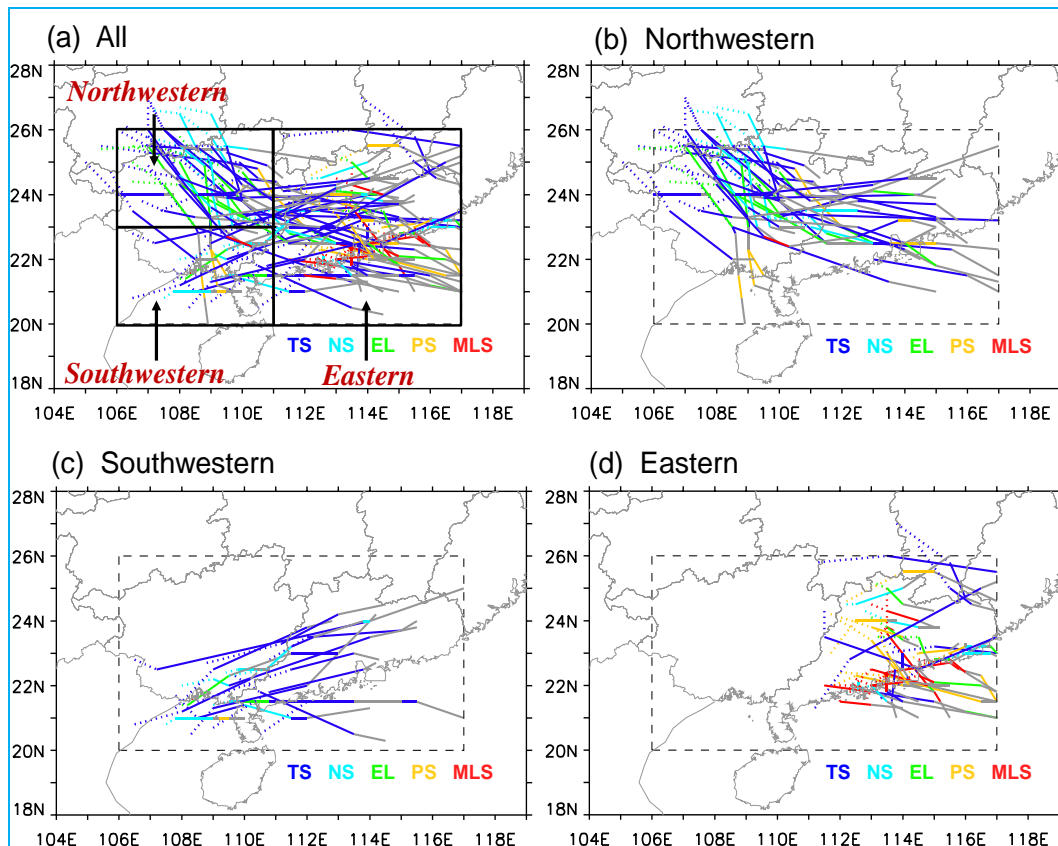
Figs 4(a-d). The tracks of (a) all the 98 MCSs observed during the pre-summer rainy season of 2013-2017 and three subsets of the MCSs formed over the (b) northwestern, (c) southwestern and (d) eastern parts of the analysis region (South China) labeled in (a), respectively. The analysis region, denoted by the dashed rectangle in panels (b)-(d), is divided into the three parts shown in (a). For each MCS, the dashed line denotes the track from its first echo to its formation and the solid line indicates the track from its formation to dissipation. The colors of each track represent the corresponding modes of the MCSs with grey representing no significant mode during the corresponding period. The grey curves demonstrate the provincial boundaries and coastlines. Reprinted from Chen *et al.* (2022), copyright 2022, with permission from Elsevier

The time of MCSs' initiation and formation exhibits distinctive spatial variations over South China. The MCSs over the northwestern part of South China (N-GX) tend to initiate in the late afternoon or evening and form around midnight, while MCSs over the southwestern part of South China (S-GX) and PRD are prone to initiate from the midnight to early morning and form in the morning. Such regional differences in the diurnal variation of MCS initiation and formation are mainly associated with two physical mechanisms. The afternoon-to-evening initiation peak over N-GX is more closely related to the thermally driven circulation associated with the heating differential between the Yunnan-Guizhou plateau (YGP) and its adjacent lower-altitude areas to the southeast. During the daytime, the YGP is warmer than the south and east areas of South China, causing upslope winds on its southeastern slope and favorable for the convection initiation over N-GX in the late afternoon, which is similar to the

mechanism governing the rainfall diurnal cycle of, *e.g.*, the Tibetan Plateau and Sichuan Basin (Bao *et al.*, 2011; Jin *et al.*, 2013). In contrast, the triggering of MCS over the PRD is closely associated with the low-level onshore winds in the boundary layer which usually reach its maximum at midnight (Du and Chen, 2019; Wang *et al.*, 2021).

The MCSs show three major moving paths after formation, also with distinctive spatial variations over South China [Fig. 4(a)]. The MCSs formed over N-GX firstly move southeasterly before reaching southeast of Guangxi [Fig. 4(b)]. Most of these MCSs then move in an easterly direction to Guangdong, with a small part of them turning southward to S-GX and Beibu Gulf. In contrast, the MCSs formed over S-GX and the coastal area of Beibu Gulf move in a northeast direction after formation [Fig. 4(c)], while the MCSs initiated along the eastern part
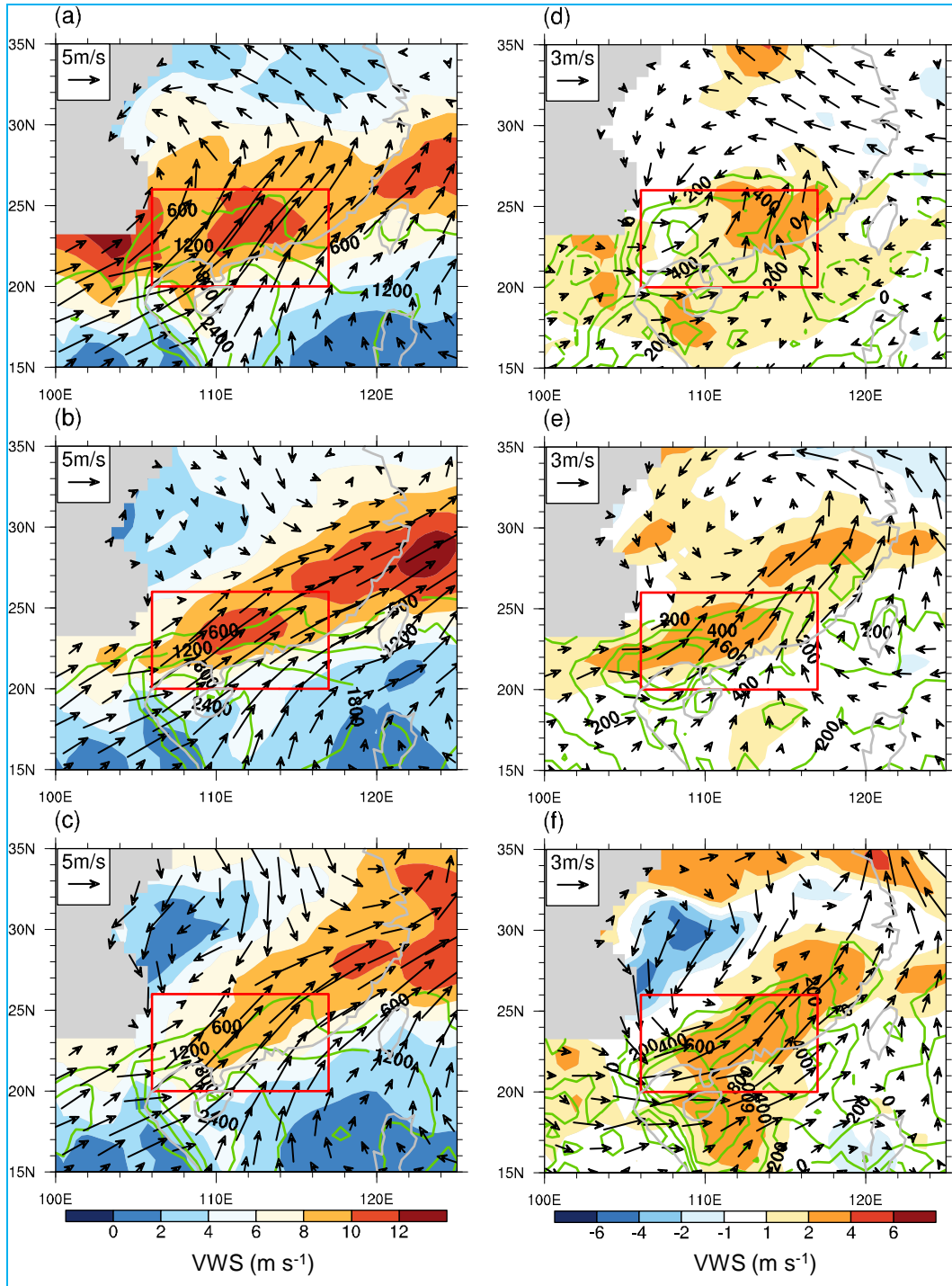
Figs. 5(a-f). (Left column) Composite analyses of the environmental conditions on the MCS days under the (a) Type-I, (b) Type-III and (c)Type-VI synoptic patterns in Fig. 10 of Chen *et al.* (2022): the vertical wind shears (VWS) between surface and 700 hPa (shadings, units: m s^{-1}), the convective available potential energy (CAPE; green contours at interval of 400 J kg^{-1}) and the wind at 850 hPa (black arrows; unit: m s^{-1}). (Right column) The differences between the MCS days and the non-MCS days under the (d) Type-I, (e) Type-III and (f) Type-VI synoptic patterns: VWS between surface and 700 hPa (shadings, units: m s^{-1}), CAPE (green contours at interval of 200 J kg^{-1}; only the positive differences are plotted) and the wind at 850 hPa (black arrows; unit: m s^{-1}). The grey-shaded regions denote the portions of isobaric surfaces underneath the ground. The grey curves demonstrate the coastlines. Reprinted from Chen *et al.* (2022), copyright 2022, with permission from Elsevier
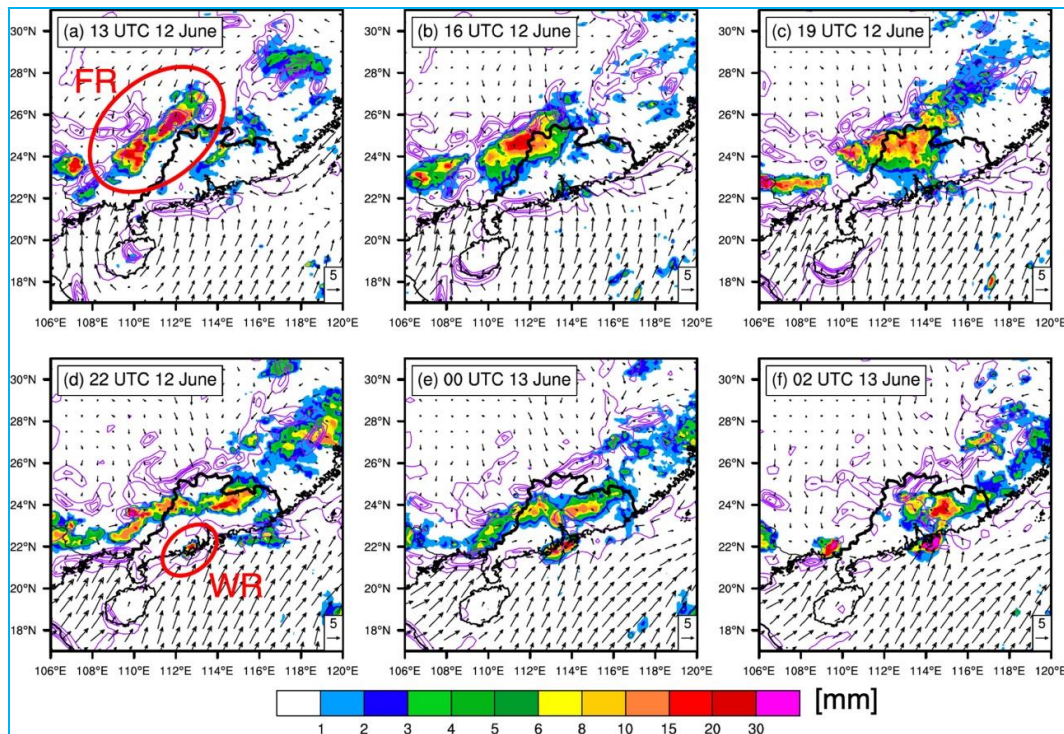
Figs. 6(a-f). The GPM IMERG hourly precipitation (color filled; mm) and front ogenesis function (purple contours; every 3×10^{-9} K m^{-1} s^{-1} starting from 2×10^{-9} K m^{-1} s^{-1}) at (a) 1300, (b) 1600, (c) 1900, (d) 2200 UTC on June 12, 2019, (e) 0000 and (f) 0200 UTC on June 13, 2019. The front ogenesis function is calculated using the surface layer data from ERA5 reanalysis data. The wind vector denotes the 10-m wind. The red ellipses in (a) and (d) show the identified frontal heavy rainfall and warm-sector heavy rainfall. Guangdong Province is outlined by thick black lines. Adapted from Han *et al.* (2021)

of South China (the coast of Guangdong and its north-central area) tend to move eastward after formation [Fig. 4(d)].

Using the obliquely rotated principal component analysis (PCA) in T mode (T-mode PCA) (Huth, 1996, 2000), Chen *et al.* (2022) classified the circulation patterns in the lower troposphere around South China during the pre-summer rainy season into six types. They found that the formation and movement characteristics of the MCSs over South China during the pre-summer rainy season are significantly governed by the synoptic conditions [Figs. 5(a-f)]. The MCSs are prone to occurrence under three [Type-I, Type-III and Type-VI; in Fig. 10 of Chen *et al.* (2022)] of the six types which feature with stronger low-level southwesterly winds than the other synoptic patterns. There are 69.2% of circulation samples and 81.8% of MCS days are under these three synoptic patterns. The analysis of the thermodynamic conditions during the MCS days under these three patterns shows that the occurrence of the MCS is accompanied with strong southwesterly low-level winds (> 10 m s^{-1}). This is consistent with previous studies showing that low-

level jets play an important role in the occurrence of MCS-producing heavy rainfall over South China(Du and Chen, 2018, 2019; Liu *et al.*, 2020). The strong southwesterly winds transport the moist and warm air from the ocean to land and establish the potentially unstable stratification over South China. The average convective available potential energy (CAPE) over South China can reach 2000 J kg^{-1} during the MCS days [Figs. 5(a-c)]. Compared with the non-MCS days, the MCS days feature positive anomalies of southwesterly wind (2-5 m s^{-1}) and CAPE (200-800 J kg^{-1}) under each synoptic pattern [Figs. 5(d-f)]. Moreover, the dynamic condition analyses by Chen et al. (2022) demonstrated that the magnitudes of vertical wind shears between surface and 700 hPa (approximately between 0-3 km) on the MCS days can reach to 8-12 m s^{-1} over South China [Figs. 5(a-c)], being favorable for the maintenance of MCSs though the cold-pool-shear relationship (Rotunno *et al.*, 1988; Weisman, 1993; Weisman and Rotunno, 2004).

Moreover, Chen *et al.* (2022) found that MCSs are prone to occur over N-GX under the synoptic pattern of Type-VI, while MCS over S-GX and PRD tend to take
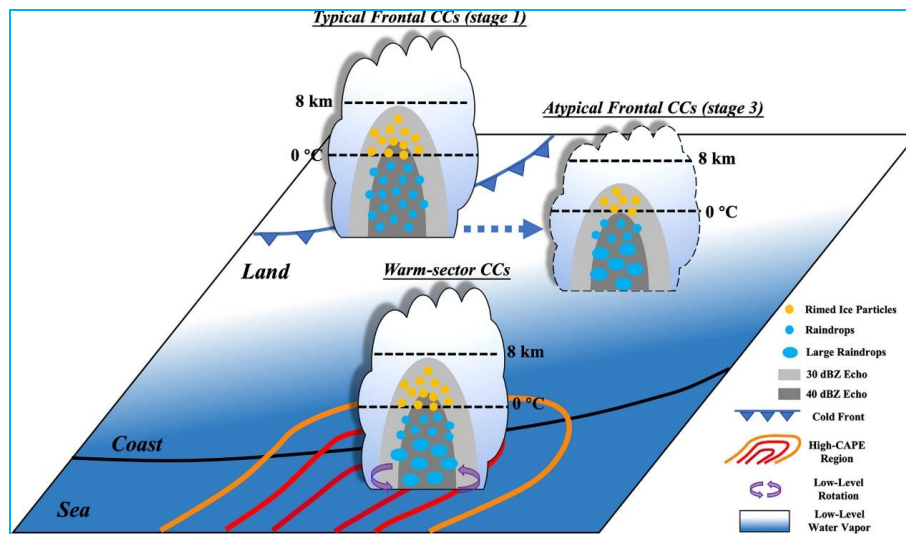
Fig. 7. Schematic diagram depicting the microphysical characteristic differences between the warm-sector convective cells and frontal convective cells at different stages and the possible influence of environmental. The grey curves demonstrate the coastlines. Adapted from Han *et al*. (2021)

place under the Type-III pattern. The decelerations of the southwesterly wind in the boundary layer appears along the coastal lines of South China under the Type-III pattern, producing a zone of synoptic-scale convergence there (not shown). Such synoptic convergence, combined with the terrain distributions and sea-land frictional contrast near the coastal lines, making this pattern favorable for the initiation and formation of MCSs over S-GX and PRD. However, the significant synoptic convergence in the lower troposphere under Type-VI appears in N-GX due to the decreasing southerly winds confronting with the northernly winds to the north, making MCSs more likely to form over N-GX under this type. After the formation, MCSs over N-GX move southeastward accompanied by the southeastward movement of the synoptic-scale convergence and under the effects of the cold-pool dynamics (Rotunno *et al*., 1988). In contrast, the mid-level wind vectors are mostly westerly under the Type-III pattern, making the MCS to move relatively more eastward due to the combined effect of the synoptic steering flows and cold-pool dynamics.

4. Microphysical characteristics

4.1. *A comparison between coexisting FR and WR*

The differences between the FR and WR in South China from the dynamical and thermodynamical perspectives have been well documented in numerous previous studies (Liu *et al*., 2020; Wu *et al*., 2020). However, their microphysical characteristics remain elusive. The recent dual-polarimetric upgrade of the

operational radar network in South China since 2016 (Zhao *et al*., 2019) has provided additional microphysical information such as particle shape, size and orientation (Zrnic and Ryzhkov, 1999). Taking advantage of large spatial coverage and high temporal resolution of the polarimetric radar observations, Han *et al*. (2021) investigated a typical heavy rainfall event during the pre-summer rainy season, featured by the coexisting FR and WR in South China.

This event occurred on June 12-13, 2019 and exhibited two coexisting rainbands, *i.e*., an inland frontal rainband and a coastal warm-sector rainband [Figs. 6(a-f)]. The inland rainband propagated southeastward to influence Guangdong province, while the coastal rainband moved along the coastline of Guangdong in the warm sector. During 1300-1600 UTC June 12, 2019, the inland rainband was close to the frontogenesis, which was identified as a surface cold front and it can be regarded as the typical FR [Figs. 6(a&b)]. Later on, the inland rainband moved away from the cold front and rebuilt ahead of the front [Figs. 6(c-e)], due to the existence of low-level convergence ahead of the front near the exit of the boundary layer jet at 950 hPa. Eventually, the FR merged with the coastal WR at about 0200 UTC on June 13, 2019 [Fig. 6(f)].

To examine the microphysical differences between the FR and WR, Han *et al*. (2021) focused on the convective cells (CCs) in the rainbands. They identified CCs based on the depth of radar reflectivity. If the points with strong radar reflectivity (>40 dBZ) exceed one-third
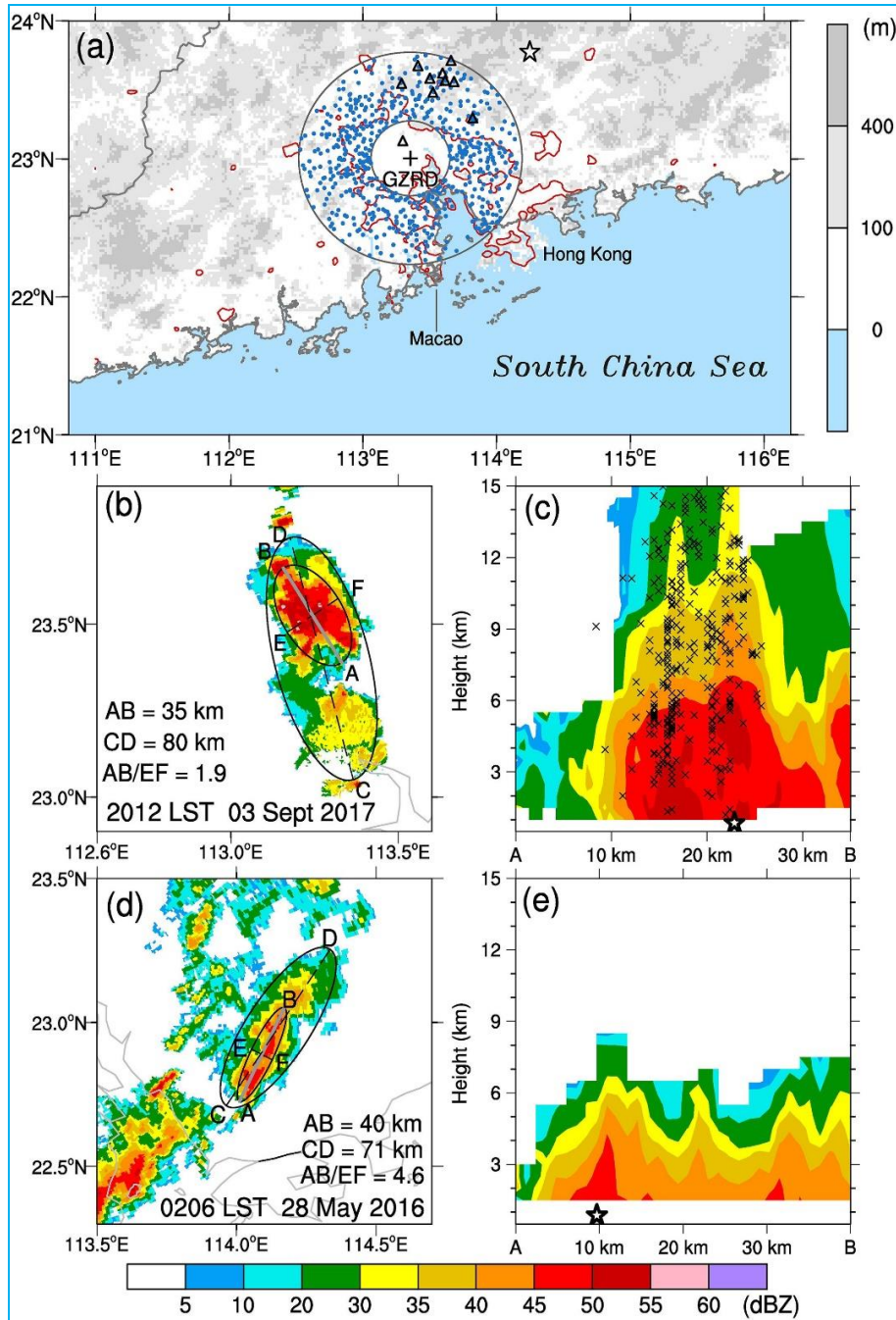
Figs. 8(a-e). (a) Topography map around the urban agglomeration in coastal South China, overlaid with the boundaries of urban areas based on the DMSP/OLS nighttime lights data in 2013 (solid red). The black plus sign represents the Guangzhou S-band dual polarization radar (GZRD) and two circles denote the 30-85 km ring zone from GZRD. Dots, triangles and the star represent rain gauges, lightning sensors and the Longmen Cloud Physics Field Experiment Base, respectively. (b) Horizontal distribution of CR (color shading) for an extreme precipitation feature (EPF) with "intense convection". Ellipses fitting ismade for the 40 dBZ and the 20 dBZ precipitation regions, respectively. The long axes are labeled as AB and CD, while the short axis of the 40 dBZ region is labeled as EF. (c) Vertical section of radar reflectivity along the line AB in (b), with a star and crosses "×" denoting positions of the near-surface extreme precipitation and the lightning pulse discharge events, respectively. (d) and (e) are the same as (b) and (c), respectively, except for an EPF of "weak convection" without lightning flashes being detected. Adapted from Yu *et al.* (2022)
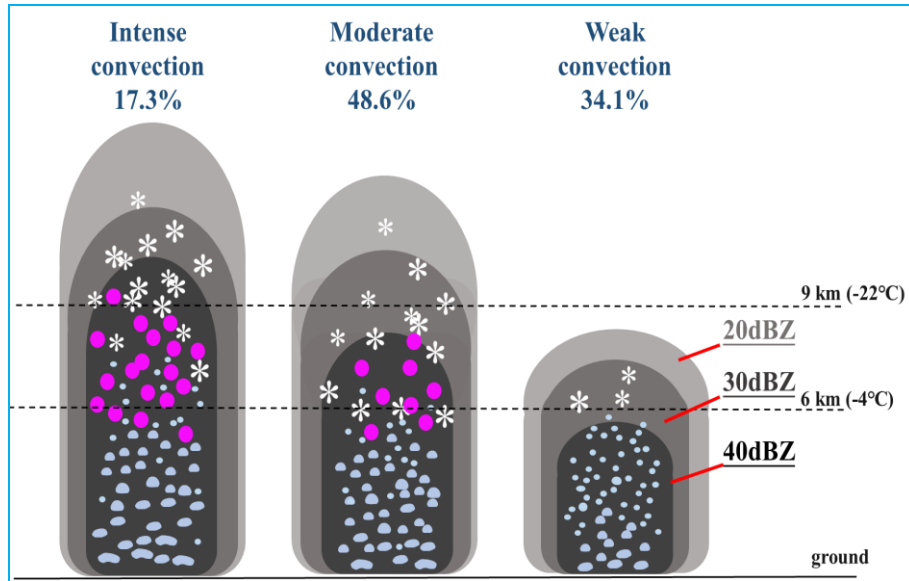
Fig. 9. Schematic diagram depicting the microphysical characteristics of extreme precipitation with the intense, moderate and weak convection, respectively, in coastal South China. Drawn based on Yu *et al*. (2022)

of the total points in each vertical column of gridded data, this column was identified as a CC. Totally 10 dual-polarimetric radars were used to provide enough samples at lower levels above 1.0-km altitude (above sea level) for robust analysis. A comprehensive analysis was conducted using the observations of radar reflectivity (Z_H), differential reflectivity (Z_{DR}) and specific differential phase (K_{DP}) and also the retrieved mass-weighted diameter (D_m) and logarithmic normalized intercept [$\log_{10}(N_W)$] for the identified frontal CCs and warm-sector CCs.

Based on their analysis results, Han *et al*. (2021) established a conceptual model (Fig. 7) and drew major conclusions as follows. (*i*) The warm-sector CCs had a larger rain-drop size and higher LWC than the frontal CCs; (*ii*) The frontal CCs near the front had more active ice-based microphysical processes with more rimed ice particles aloft, compare to the later stage when they were organized again ahead of the front; (*iii*) The raindrop size of frontal CCs near the front was smaller than that of the frontal CCs ahead of the front. In their discussions about possible reasons for the microphysical differences between FR and WR, Han *et al*. (2021) speculated that the higher low-level humidity in the warm sector and the more evident low-level meso-γ-scale rotation for the WR CCs could promote warm rain microphysical processes and large raindrops could result from active warm rain processes even with relatively inactive ice-based processes.

4.2. *Microphysical characteristics of extreme rainfall over the PRD*

Extreme short-term(one to a few hours) rainfall accumulation occasionally occurs over monsoon coastal areas and tends to occur more frequently with additional warming (Chen *et al*., 2018). In South China, hourly rainfall accumulations beyond 100 mm are not unusual. In the record-breaking rainfall event influencing Guangzhou on May 7, 2017 (referred to as *Guangzhou May 7event* hereafter), the maximum 60-min rainfall accumulation at about 06 LT reached 219 mm. Using integrated multi platform observations, particularly dual polarization radar measurements and a four-dimensional variational Doppler radar analysis system, Li *et al*. (2021) demonstrated that the extreme rainfall was produced by a quasi-stationary storm, facilitated by weak environmental flows and a convectively generated weak cold pool. The maximum hourly rainfall was associated with active warm-rain (but weak mixed-phase) microphysical processes, with raindrop size distribution (RSD) closer to marine convection. Production of such extreme hourly rainfall was accompanied by a low-level meso-γ-scale vortex due to stretching of intense latent heating-induced convergence, which, in turn, helps organize convective updrafts into its core region. Interestingly, another rainstorm with much stronger convective intensity developed several hours earlier and produced maximum hourly rainfall of about 120 mm h^{-1}, *i.e*., the stronger convection produced relatively less extreme rainfall.

Yu *et al*. (2022) utilized 2-year observations from the Guangzhou dual-polarization radar, distrometers and lightning sensors to investigate microphysical processes in extreme rainfall-producing convective cores (locations of the instruments are shown in Fig. 8(a). They defined an extreme precipitation feature (EPF) as a contiguous area of strong composite reflectivity ($\geq$ 40 dBZ) which consists of at least 51 pixels and contains at least 0.5 km^2 contiguous area of an extreme instantaneous rain rate (> 114 mm h^{-1}). With this definition, 9292 EPFs were identified from the Guangzhou radar observations at 6 min intervals. Two examples are shown in Figs. 8(b-e). Convective intensity of each EPF was estimated using the maximum height of 40-dBZ echo (maxHt_40dBZ). A wide range of convective intensity was found in the EPFs. About 17.3% and 34.1% EPFs have maxHt_40dBZ beyond 9 km ("intense convection") and below 6 km ("weak convection"), respectively, with 48.6% EPFs having maxHt_40dBZ between 6-9 km ("moderate convection"). These results indicate a low correlation between convective intensities and instantaneous rain rates, which is not only consistent with previous finding of a low overlap between extreme convection and extreme rainfall in the subtropics and tropics (Hamada *et al*., 2014, 2015), but also advances our understanding of the probability distribution of convective intensity that produces extreme rainfall in the monsoon coastal areas.

Characteristics of microphysical processes leading to the generation of extreme rainfall in monsoon coastal areas are quantified for the first time in a statistical sense by Yu *et al*. (2022). Overall, warm-rain microphysical processes contribute significantly to the production of extreme rainfall, with dominance of the coalescence in the liquid-phase processes, mean raindrop size slightly larger than the "maritime" regime and mean concentration one order of magnitude higher than the "continental" regime (Bringi *et al*., 2003). Compared to the EPFs with stronger convection, the EPFs with weaker convective intensity are characterized by a larger ratio of liquid water path to ice water path (indicating a larger contribution from warm rain processes), smaller raindrop size, reduced raindrop mass and weakened size sorting and less breakup of large raindrops. We establish a conceptual model to schematically depict the major findings of Yu *et al*. (2022) (Fig. 9).

5.   Concluding remarks

To conclude, this article highlights new insights obtained in the past 3-4 years on heavy rainfall in a typical monsoon coastal area (South China) from the microphysical perspective and also on the associated CI and MCSs in a statistical sense, many of which we have yet to understand. More studies are therefore necessary to improve our understanding, which will help improve prediction of heavy rainfall events. The following issues are suggested for future studies on heavy rainfall over South China.

(*i*)   To analyze general features of MCSs and sub MCSs (horizontal span of about 20-100 km) during the later rainy season in South China (July to September) and their association with disturbances of synoptic and subsynoptic scales.

(*ii*)   To compare microphysical characteristics between the FR and WR using a large number of cases and analyze possible reasons for their differences from the aspects of environmental conditions and storm internal dynamics.

(*iii*) To investigate the convective intensity and microphysical features in extreme rainfall accumulations over a range of time scales, *i.e*., from minutes to hourly and a few hours.

(*iv*) To analyze the low-level meso-γ-scale vortices accompanying extreme short-term precipitation (*e.g*., hourly) and quantify the contribution of low-level rotation to rainfall intensification.

Disclaimer : The contents and views expressed in this study are the views of the authors and do not necessarily reflect the views of the organizations they belong to.

References

Aves, S. L. and Johnson, R. H., 2008, "The diurnal cycle of convection over the Northern South China sea", *Journal of the Meteorological Society of Japan*, **86**, 919-934. doi : 10.2151/jmsj.86.919.

Bai, L., Chen, G. and Huang, L., 2020b, "Convection Initiation in Monsoon Coastal Areas (South China)", *Geophysical Research Letters*, **47**, 1-11. doi : 10.1029/2020GL087035.

Bai, L., Chen, G. and Huang, L., 2020a, "Image processing of radar mosaics for the climatology of convection initiation in South China", *Journal of Applied Meteorology and Climatology*, **59**, 65–81. doi : 10.1175/JAMC-D-19-0081.1.

Bao, X., Luo, Y. and Gao, X., 2021, "The Synoptic Impacts on the Convection Initiation of a Warm-Sector Heavy Rainfall Event Over Coastal South China Prior to the Monsoon Onset: A Numerical Modeling Study", *Journal of Geophysical Research: Atmospheres*, **126**. doi : 10.1029/2020JD034335.

Bao, X., Zhang, F. and Sun, J., 2011, "Diurnal variations of warm-season precipitation east of the Tibetan Plateau over China", *Monthly Weather Review*, **139**, 2790-2810. doi : 10.1175/MWR-D-11-00006.1.

Bringi, V. N., Chandrasekar, V., Hubbert, J., Gorgucci, E., Randeu, W. L. and Schoenhuber, M., 2003, "Raindrop size distribution in different climatic regimes from disdrometer and dual-polarized radar analysis", *Journal of the Atmospheric Sciences*, **60**, 354-365. doi : 10.1175/1520-0469(2003)060<0354:RSDIDC> 2.0.CO;2

Chen, Y., Moufouma-Okia, W., Masson-Delmotte, V., Zhai, P. and Pirani, A., 2018, "Recent progress and emerging topics on weather and climate extremes since the fifth assessment report of the intergovernmental panel on climate change", *Annual Review of Environment and Resources*, **43**, 35-59. doi : 10.1146/annurev-environ-102017-030052.

Chen, T. C., Wang, S. Y., Huang, W. R. and Yen, M. C., 2004, "Variation of the East Asian summer monsoon rainfall", *Journal of Climate*, **17**, 744-762. doi : 10.1175/1520-0442(2004)017< 0744:VOTEAS>2.0.CO;2.

Chen, G., Lan, R., Zeng, W., Pan, H. and Li, W., 2018, "Diurnal variations of rainfall in surface and satellite observations at the Monsoon Coast (South China)", *Journal of Climate*, **31**, 1703-1724. doi : 10.1175/JCLI-D-17-0373.1.

Chen, X., Zhang, F. and Zhao, K., 2016, "Diurnal variations of the land-sea breeze and its related precipitation over south China", *Journal of the Atmospheric Sciences*, **73**, 4793-4815. doi : 10.1175/JAS-D-16-0106.1.

Chen, Y., Luo, Y. and Liu, B., 2022, "General features and synoptic-scale environments of mesoscale convective systems over South China during the 2013-2017 pre-summer rainy seasons", *Atmospheric Research*, **266**, 105954. doi : 10.1016/j.atmosres.2021.105954.

Ding, Y. H., 1994, "Monsoons over China", *Monsoons over China*, 7923. doi : 10.1007/bf02666553.

Ding, Y. H. and Chan, J. C. L., 2005, "The East Asian summer monsoon: An overview", *Meteorology and Atmospheric Physics*, **89**, 117-142. doi : 10.1007/s00703-005-0125-z.

Du, Y. and Chen, G., 2018, "Heavy rainfall associated with double low-level jets over southern China. Part I: Ensemble-based analysis", *Monthly Weather Review*, **146**, 3827-3844. doi : 10.1175/MWR-D-18-0101.1.

Du, Y. and Chen, G., 2019, "Climatology of low-level jets and their impact on rainfall over southern China during the early-summer rainy season", *Journal of Climate*, **32**, 8813-8833. doi : 10.1175/JCLI-D-19-0306.1.

Du, Y., Chen, G., Han, B., Mai, C., Bai, L. and Li, M., 2020a, "Convection initiation and growth at the coast of South China. Part I: Effect of the marine boundary layer jet", *Monthly Weather Review*, **148**, 3847-3869. doi : 10.1175/MWR-D-20-0089.1.

Du, Y., Chen, G., Han, B., Bai, L. and Li, M., 2020b, "Convection initiation and growth at the coast of south China. part II: Effects of the terrain, coastline and cold pools", *Monthly Weather Review*, **148**, 3871-3892. doi : 10.1175/MWR-D-20-0090.1.

Huang, S., Li, Z. and Bao, C., 1986, "Heavy Rains in the First Rainy Season of South China", *Guangdong Science and Technology Press*, 230 (in Chinese).

Huang, Z., Zhang, D. and Lin, L. X., 2005, "Synoptic analysis of heavy rain related to monsoon trough in the latter flood season of Guangdong", *Meteorology Monthly*, **31**, 19-24. doi : 10.3969/j.issn.1000-0526.2005.09.004. (in Chinese).

Hamada, A., Murayama, Y. and Takayabu, Y. N., 2014, "Regional characteristics of extreme rainfall extracted from TRMM PR measurements", *Journal of Climate*, **27**, 8151-8169. doi : 10.1175/JCLI-D-14-00107.1.

Hamada, A., Takayabu, Y. N., Liu, C. and Zipser, E. J., 2015, "Weak linkage between the heaviest rainfall and tallest storms", *Nature Communications*, **6**, 1-6. doi : 10.1038/ncomms7213.

Han, B., Du, Y., Wu, C. and Liu, X., 2021, "Microphysical Characteristics of the Coexisting Frontal and Warm-Sector Heavy Rainfall in South China", *Journal of Geophysical Research : Atmospheres*, **126**, 1-24, doi : 10.1029/2021JD 035446

Houze, R. A., Jr., Geotis, S. G., Marks, F. D., Jr. and West, A. K., 1981, "Winter Monsoon Convection in the Vicinity of North Borneo. Part I : Structure and Time Variation of the Clouds and Precipitation", *Monthly Weather Review*, **109**, 1595-1614. doi : 10.1175/1520-0493(1981)109<1595:WMCITV>2.0.CO;2.

Houze, R. A. Jr., Wilton, D. C. and Smull, B. F., 2007, "Monsoon convection in the Himalayan region as seen by the TRMM Precipitation Radar", *Quarterly Journal of the Royal Meteorological Society*, **133**, 1389-1411. doi : 10.1002/qj.

Houze Jr., R. A., 2018, "100 years of research on mesoscale convective systems", *Meteorological Monographs*, **59**, 17.1-17.54. doi : 10.1175/AMSMONOGRAPHS-D-18-0001.1.

Huth, R., 1996, "Properties of the circulation classification scheme based on the rotated principal component analysis", *Meteorology and Atmospheric Physics*, **59**, 217-233. doi : 10.1007/BF01030145.

Huth, R., 2000, "A circulation classification scheme applicable in GCM studies", *Theoretical and Applied Climatology*, **67**, 1-18. doi : 10.1007/s007040070012.

Hong, W. and Ren, X., 2013, "Persistent heavy rainfall over South China during May-August : Subseasonal anomalies of circulation and sea surface temperature", *Acta Meteorologica Sinica*, **27**, 769-787. doi : 10.1007/s13351-013-0607-8.

Jin, X., Wu, T. and Li, L., 2013, "The quasi-stationary feature of nocturnal precipitation in the Sichuan Basin and the role of the Tibetan Plateau", *Climate Dynamics*, **41**, 977-994. doi : 10.1007/s00382-012-1521-y.

Li, J., Li, N. and Yu, R., 2019, "Regional differences in hourly precipitation characteristics along the western coast of south China", *Journal of Applied Meteorology and Climatology*, **58**, 2717-2732. doi : 10.1175/JAMC-D-19-0150.1.

Li, M., Luo, Y., Zhang, D. L., Chen, M., Wu, C., Yin, J. and Ma, R., 2021, "Analysis of a Record-Breaking Rainfall Event Associated with a Monsoon Coastal Megacity of South China Using Multisource Data", *IEEE Transactions on Geoscience and Remote Sensing*, **59**, 6404-6414. doi : 10.1109/ TGRS.2020.3029831

Li, Z., Luo, Y., Du, Y. and Chen, Y., 2020, "Statistical characteristics of presummer rainfall over South China and associated synoptic conditions", *J. Meteor. Soc. Japan*, **98**, 213-233. doi : 10.2151/jmsj.2020-012.

Liu, X., Luo, Y., Guan, Z. and Zhang, D. L., 2018, "An Extreme Rainfall Event in Coastal South China During SCMREX-2014: Formation and Roles of Rainb and Echo Trainings", *Journal of Geophysical Research: Atmospheres*, **123**, 9256-9278. doi : 10.1029/2018JD028418.

Liu, X., Luo, Y., Huang, L., Zhang, D. L. and Guan, Z., 2020, "Roles of Double Low-Level Jets in the Generation of Coexisting Inland and Coastal Heavy Rainfall Over South China During the Presummer Rainy Season", *Journal of Geophysical Research: Atmospheres*, **125**, 1-23. doi : 10.1029/2020JD032890.

Luo, Y., Sun, J., Li, Y., Xia, R., Du, Y., Yang, S., Zhang, Y., Chen, J., Dai, K., Shen, X., Chen, H., Zhou, F., Liu, Y., Fu, S., Wu, M., Xiao, T., Chen, Y., Li, H. and Li, M., 2020, "Science and Prediction of Heavy Rainfall over China : Research Progress since the Reform and Opening-Up of New China", In *Journal of Meteorological Research* (Vol. 34, Issue 3) doi : 10.1007/s13351-020-0006-x.

Luo, Y., Wang, H., Zhang, R., Qian, W. and Luo, Z., 2013, "Comparison of Rainfall Characteristics and Convective Properties of Monsoon Precipitation Systems over South China and the Yangtze and Huai River Basin", *Journal of Climate*, **26**, 110-132. doi : 10.1175/JCLI-D-12-00100.1.

Luo, Y., Zhang, R., Wan, Q., Wang, B., Wong, W. K., Hu, Z., Jou, B. J. D., Lin, Y., Johnson, R. H., Chang, C. P., Zhu, Y., Zhang, X., Wang, H., Xia, R., Ma, J., Zhang, D. L., Gao, M., Zhang, Y., Liu, X. and Xiao, Y., 2017, "The southern China monsoon rainfall experiment (SCMREX)", *Bulletin of the American Meteorological Society*, **98**, 999-1013. doi : 10.1175/BAMS-D-15-00235.1.

Meng, Z., Yan, D. and Zhang, Y., 2013, "General features of squall lines in East China", *Monthly Weather Review*, **141**, 1629-1647. doi : 10.1175/MWR-D-12-00208.1.

Meng, W. and Wang, Y., 2016, "A diagnostic study on heavy rainfall induced by typhoon utor (2013) in South China: 1. Rainfall asymmetry at landfall", *Journal of Geophysical Research*, **121**, 12,781-12,802. doi : 10.1002/2015JD024646.

Ni, Y. Q. and Zhou, X. J., 2006, "Main scientific issues and achievements of state 973 Project on study for formation mechanism and prediction theories of severe weather disasters in China", *Advances in Earth Science*, **21**, 881-894 (in Chinese).

Qian, W. and Lee, D. K., 2000, "Seasonal March of Asian summer monsoon", *International Journal of Climatology*, **20**, 1371-1386. doi : 10.1002/1097-0088(200009)20:11<1371::AID-JOC538>3.0.CO;2-V.

Parker, M. D. and Johnson, R. H., 2000, "Organizational modes of midlatitude mesoscale convective systems", *Monthly Weather Review*, **128**, 3413-3436. doi : 10.1175/1520-0493(2001)129<3413:OMOMMC>2.0.CO;2.

Ramage, C. S., 1952, "Variation of Rainfall Over South China Through the Wet Season", *Bulletin of the American Meteorological Society*, **33**, 308-311. doi : 10.1175/1520-0477-33.7.308.

Rotunno, R., Klemp, J. B. and Weisman, M., 1988, "A theory for strong, long-lived squall lines", *Journal of Atmospheric Sciences*, **45**, 463-485. doi : 10.1175/1520-0469(1988)045<0463:ATFSLL>2.0.CO;2.

Roca, R., Aublanc, J., Chambon, P., Fiolleau, T. and Viltard, N., 2014, "Robust observational quantification of the contribution of mesoscale convective systems to rainfall in the tropics", *Journal of Climate*, **27**, 4952-4958. doi : 10.1175/JCLI-D-13-00628.1.

Shepherd, J. M., 2005, "A review of current investigations of urban-induced rainfall and recommendations for the future", *Earth Interactions*, **9**, doi : 10.1175/EI156.1.

Schumacher, R. S. and Rasmussen, K. L., 2020, "The formation, character and changing nature of mesoscale convective systems", *Nature Reviews Earth and Environment*, **1**, 300-314. doi : 10.1038/s43017-020-0057-7.

Sun, X., Luo, Y., Gao, X., Wu, M., Li, M., Huang, L., Zhang, D. L. and Xu, H., 2021, "On the localized extreme rainfall over the great bay area in South China with complex topography and strong UHI effects", *Monthly Weather Review*, **149**, 2777-2801. doi : 10.1175/MWR-D-21-0004.1.

Virtsa, K. S. and Houze, R. A., 2016, "Seasonal and intraseasonal variability of mesoscale convective systems over the South Asian monsoon region", *Journal of the Atmospheric Sciences*, **73**, 4753-4774. doi : 10.1175/JAS-D-16-0022.1.

Wang, C., Zhao, K., Huang, A., Chen, X. and Rao, X., 2021, "The crucial role of synoptic pattern in determining the spatial distribution and diurnal cycle of heavy rainfall over the south china coast", *Journal of Climate*, **34**, 2441-2458. doi : 10.1175/JCLI-D-20-0274.1.

Wang, H., Luo, Y. and Jou, B. J. D., 2014, "Initiation, maintenance and properties of convection in an extreme rainfall event during SCMREX: Observational analysis", *Journal of Geophysical Research*, **119**, 13,206-13,232. doi : 10.1002/2014JD022339.

Weisman, M. L., 1993, "The genesis of severe, long-lived bow echoes", *Journal of the Atmospheric Sciences*, **50**, 645-670. doi : 10.1175/1520-0469(1993)050<0645:TGOSLL>2.0.CO;2.

Weisman, M. L. and Rotunno, R., 2004, "'A theory for strong long-lived squall lines' revisited", *Journal of the Atmospheric Sciences*, **61**, 361–382. doi : 10.1175/1520-0469(2004)061<0361:ATFSLS>2.0.CO;2.

Wu, M. and Luo, Y., 2016, "Mesoscale observational analysis of lifting mechanism of a warm-sector convective system producing the maximal daily precipitation in China mainland during pre-summer rainy season of 2015", *Journal of Meteorological Research*, **30**, 719-736. doi : 10.1007/s13351-016-6089-8.

Wu, M., Luo, Y., Chen, F. and Wong, W. K., 2019, "Observed link of extreme hourly precipitation changes to urbanization over coastal South China", *Journal of Applied Meteorology and Climatology*, **58**, 1799-1819. doi : 10.1175/JAMC-D-18-0284.1.

Wu, N., Ding, X., Wen, Z., Chen, G., Meng, Z., Lin, L. and Min, J., 2020, "Contrasting frontal and warm-sector heavy rainfalls over South China during the early-summer rainy season", *Atmospheric Research*, **235**, 104693. doi : 10.1016/j.atmosres.2019.104693.

Xie, S. P., Xu, H., Saji, N. H., Wang, Y. and Liu, W. T., 2006, "Role of narrow mountains in large-scale organization of Asian Monsoon convection", *Journal of Climate*, **19**, 3420-3429. doi : 10.1175/JCLI3777.1.

Xu, W., Zipser, E. J. and Liu, C., 2009, "Rainfall characteristics and convective properties of mei-yu precipitation systems over South China, Taiwan and the South China Sea. Part I : TRMM observations", *Monthly Weather Review*, **137**, 4261-4275.

Yuan, F., Wei, K., Chen, W., Fong, S. K. and Leong, K. C, 2010, "Temporal Variations of the Frontal and Monsoon Storm Rainfall during the First Rainy Season in South China", *Atmospheric and Oceanic Science Letters*, **3**, 243-247. doi : 10.1080/16742834.2010.11446876.

Yin, J., Zhang, D. L., Luo, Y. and Ma, R., 2020, "On the extreme rainfall event of 7 May 2017 over the Coastal City of Guangzhou. Part I: Impacts of urbanization and orography", *Monthly Weather Review*, **148**, 955-979. doi : 10.1175/MWR-D-19-0212.1.

Yu, S., Luo, Y., Wu, C., Zheng, D., Liu, X. and Xu, W., 2022, "Convective and Microphysical Characteristics of Extreme Precipitation Revealed by Multisource Observations Over the Pearl River Delta at Monsoon Coast", *Geophysical Research Letters*, **49**, e2021GL097043, doi: 10.1029/2021GL097043

Zeng, Z. and Wang, D., 2022, "On the local rain rate extreme associated with a mesovortex over South China : Observational structures, characteristics and evolution", *Monthly Weather Review*, **150**, 1075-1096. doi : 10.1175/MWR-D-21-0033.1.

Zhou, X., 2003, "Heavy rainfall experiment in South China during pre-rainy season (HUAMEX)", *China Meteorological Press, Beijing,* 220pp. (in Chinese).

Zhang, R., Ni, Y., Liu, L., Luo, Y. and Wang, Y., 2011, "South China heavy rainfall experiments (SCHeREX)", *Journal of the Meteorological Society of Japan*, **89**, 153-166. doi : 10.2151/jmsj.2011-A10.

Zhao, K., Huang, H., Wang, M., Lee, W. C., Chen, G., Wen, L., Wen, J., Zhang, G., Xue, M., Yang, Z., Liu, L., Wu, C., Hu, Z. and Chen, S., 2019, "Recent Progress in Dual-Polarization Radar Research and Applications in China", *Advances in Atmospheric Sciences*, **36**, 961-974. doi : 10.1007/s00376-019-9057-2.

Zrnic, D. S. and Ryzhkov, A. V., 1999, "Polarimetry for Weather Surveillance Radars", *Bulletin of the American Meteorological Society*, **80**, 389-406. doi : 10.1175/1520-0477(1999)080<0389: PFWSR>2.0.CO;2.